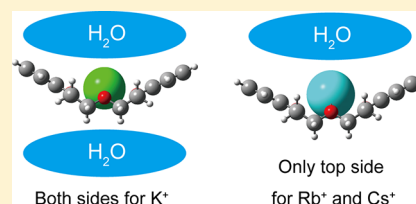


Microhydration of Dibenzo-18-Crown-6 Complexes with  $K^+$ ,  $Rb^+$ , and  $Cs^+$  Investigated by Cold UV and IR Spectroscopy in the Gas PhaseYoshiya Inokuchi,<sup>\*,†</sup> Takayuki Ebata,<sup>†</sup> and Thomas R. Rizzo<sup>‡</sup><sup>†</sup>Department of Chemistry, Graduate School of Science, Hiroshima University, Higashi-Hiroshima, Hiroshima 739-8526, Japan<sup>‡</sup>Laboratoire de Chimie Physique Moléculaire, École Polytechnique Fédérale de Lausanne, Lausanne CH-1015, Switzerland

## Supporting Information

**ABSTRACT:** In this Article, we examine the hydration structure of dibenzo-18-crown-6 (DB18C6) complexes with  $K^+$ ,  $Rb^+$ , and  $Cs^+$  ion in the gas phase. We measure well-resolved UV photodissociation (UVPD) spectra of  $K^+ \cdot DB18C6 \cdot (H_2O)_n$ ,  $Rb^+ \cdot DB18C6 \cdot (H_2O)_n$ , and  $Cs^+ \cdot DB18C6 \cdot (H_2O)_n$  ( $n = 1-8$ ) complexes in a cold, 22-pole ion trap. We also measure IR-UV double-resonance spectra of the  $Rb^+ \cdot DB18C6 \cdot (H_2O)_{1-5}$  and the  $Cs^+ \cdot DB18C6 \cdot (H_2O)_3$  complexes. The structure of the hydrated complexes is determined or tentatively proposed on the basis of the UV and IR spectra with the aid of quantum chemical calculations. Bare complexes ( $K^+ \cdot DB18C6$ ,  $Rb^+ \cdot DB18C6$ , and  $Cs^+ \cdot DB18C6$ ) have a similar boat-type conformation, but the distance between the metal ions and the DB18C6 cavity increases with increasing ion size from  $K^+$  to  $Cs^+$ . Although the structural difference of the bare complexes is small, it highly affects the manner in which each is hydrated. For the hydrated  $K^+ \cdot DB18C6$  complexes, water molecules bind on both sides (top and bottom) of the boat-type  $K^+ \cdot DB18C6$  conformer, while hydration occurs only on top of the  $Rb^+ \cdot DB18C6$  and  $Cs^+ \cdot DB18C6$  complexes. On the basis of our analysis of the hydration manner of the gas-phase complexes, we propose that, for  $Rb^+ \cdot DB18C6$  and  $Cs^+ \cdot DB18C6$  complexes in aqueous solution, water molecules will preferentially bind on top of the boat conformers because of the displaced position of the metal ions relative to DB18C6. In contrast, the  $K^+ \cdot DB18C6$  complex can accept  $H_2O$  molecules on both sides of the boat conformation. We also propose that the characteristic solvation manner of the  $K^+ \cdot DB18C6$  complex will contribute entropically to its high stability and thus to preferential capture of  $K^+$  ion by DB18C6 in solution.



## 1. INTRODUCTION

Crown ethers are the most common host molecules for ion complexation in supramolecular and organic chemistry.<sup>1</sup> One of their characteristics is the ability to selectively encapsulate certain metal ions. For example, dibenzo-18-crown-6 (DB18C6) selectively captures  $K^+$  among alkali metal ions in aqueous solution.<sup>2,3</sup> One important conclusion derived from our previous studies of ion–crown ether complexes<sup>4–6</sup> is that solvent effects highly control the alkali ion selectivity. In addition, a number of studies suggest the existence of multiple isomers,<sup>7–11</sup> which contributes to the complex stability. In our previous work, we examined the number and the structure of isomers in bare and microsolvated forms of crown ether complexes by gas-phase spectroscopy and found their relation to the guest selectivity.<sup>4–6,12–15</sup> We determined the structure of DB18C6 complexes with alkali metal ions,  $M^+ \cdot DB18C6$  ( $M = Li, Na, K, Rb$ , and  $Cs$ ), using UV and IR spectroscopy under cold gas-phase conditions.<sup>4</sup> In bare  $K^+ \cdot DB18C6$ ,  $Rb^+ \cdot DB18C6$ , and  $Cs^+ \cdot DB18C6$ , the DB18C6 part adopts a similar boat-type open conformation, but the distance between the DB18C6 cavity and the metal ions increases with increasing ion size from  $K^+$  to  $Cs^+$ .<sup>4</sup> For microhydrated systems, we reported UV and IR spectra of hydrated  $K^+ \cdot DB18C6$  complexes,  $K^+ \cdot DB18C6 \cdot (H_2O)_{1-5}$ , in the gas phase.<sup>6</sup> Because the  $K^+$  ion in the  $K^+ \cdot DB18C6$  complex is encapsulated deeply with the crown cavity,  $H_2O$  molecules can bind directly to the  $K^+$  ion on both (top

and bottom) sides of the boat-type  $K^+ \cdot DB18C6$  conformer. This hydration manner is due to the optimum matching in size between the DB18C6 cavity and the  $K^+$  ion.

In the present work, we extend our investigation of hydrated complexes to larger alkali-metal ions, that is,  $Rb^+ \cdot DB18C6$  and  $Cs^+ \cdot DB18C6$  complexes. As mentioned above, bare  $K^+ \cdot DB18C6$ ,  $Rb^+ \cdot DB18C6$ , and  $Cs^+ \cdot DB18C6$  complexes have a similar boat-type structure, but the position of the metal ions with respect to the DB18C6 part is slightly different from each other.<sup>4</sup> We examine how the difference in the metal position, or difference in the matching in size between the DB18C6 cavity and the metal ions, affects the manner of hydration.

## 2. EXPERIMENTAL AND COMPUTATIONAL METHODS

The details of our experimental approach have been given elsewhere.<sup>4,6,16</sup> Briefly, the  $K^+ \cdot DB18C6 \cdot (H_2O)_n$ ,  $Rb^+ \cdot DB18C6 \cdot (H_2O)_n$ , and  $Cs^+ \cdot DB18C6 \cdot (H_2O)_n$  ( $n = 1-8$ ) complexes are produced continuously at atmospheric pressure via nano-electrospray of a solution containing KCl, RbCl, or CsCl and DB18C6 ( $\sim 10 \mu M$  each) dissolved in methanol/water ( $\sim 9:1$  volume ratio). The parent ions of interest are selected in a quadrupole mass filter and injected into a 22-pole RF ion trap,

Received: December 16, 2017

Revised: March 20, 2018

Published: March 27, 2018



which is cooled by a closed-cycle He refrigerator to 6 K. The trapped ions are cooled internally and translationally to  $\sim 10$  K through collisions with cold He buffer gas,<sup>4,16–18</sup> which is pulsed into the trap. The trapped ions are then irradiated with a UV laser pulse, which causes some fraction of them to dissociate. The resulting charged photofragments, as well as the remaining parent ions, are released from the trap, mass-analyzed by a second quadrupole, and detected with a channeltron electron multiplier. Ultraviolet photodissociation (UVPD) spectra of parent ions are obtained by plotting the yield of the photofragment ion as a function of the UV laser wavenumber. The UVPD spectra of the  $M^+\cdot\text{DB18C6}\cdot(\text{H}_2\text{O})_n$  ( $M = \text{K}, \text{Rb}, \text{and Cs}$ ) complexes are measured by monitoring the yield of the bare  $M^+\cdot\text{DB18C6}$  photofragment ion, because it is a dominant photodissociation product and is hardly affected by the metastable decay of the parent ions between the first quadrupole and the 22-pole ion trap. For IR-UV double-resonance spectroscopy, the output pulse of an IR optical parametric oscillator (OPO) precedes the UV pulse by  $\sim 100$  ns and counter-propagates collinearly with it through the 22-pole trap. Absorption of the IR light by the ions warms them up, modifying their absorption.<sup>19</sup> We obtain IR-UV depletion and gain spectra by tuning the wavenumber of the UV laser either to the vibronic transition of a specific conformer or to a nonresonant position, respectively. The IR-UV depletion spectra provide conformer-selective IR spectra, whereas the IR-UV gain spectra represent the overall IR absorption due to all the isomers present in the experiment.

For geometry optimization of the  $M^+\cdot\text{DB18C6}\cdot(\text{H}_2\text{O})_n$  ( $M = \text{K}, \text{Rb}, \text{and Cs}$ ) complexes, we first use a classical force field to find conformational minima. The initial conformational search is performed by using the mixed torsional search with low-mode sampling and the AMBER\* force field as implemented in MacroModel version 9.1.<sup>20</sup> Minimum-energy conformers found with the force field calculations are then optimized at the M05-2X/6-31+G(d) level and successively at the M05-2X/6-311++G(d,p) level using the GAUSSIAN09 program package.<sup>21</sup> Vibrational analysis is carried out for the optimized structures at the M05-2X/6-311++G(d,p) level. Calculated frequencies at the M05-2X/6-311++G(d,p) level are scaled with a factor of 0.9425 for comparison with the IR-UV spectra. This factor was determined so as to simulate the IR spectrum of the  $\text{K}^+\cdot\text{DB18C6}\cdot(\text{H}_2\text{O})_1$  complex.<sup>6</sup> All stable conformers are named systematically using “Rb1a” notation, where the first letters indicate the metal ion of a complex, the subsequent number represents the number of the attached  $\text{H}_2\text{O}$  molecules, and the final lower case letter stands for the stability order of conformers determined at the M05-2X/6-311++G(d,p) level with zero-point energy correction. For Rb and Cs, we use the Stuttgart RLC as effective core potentials (ECPs); functions of the ECPs are obtained from a database of basis sets.<sup>22</sup>

### 3. RESULTS

**3.1. UVPD Spectra.** Figure S1 of the Supporting Information displays the UVPD spectra of the  $\text{K}^+\cdot\text{DB18C6}\cdot(\text{H}_2\text{O})_n$  ( $n = 0–8$ ) complexes in the 35 800–36 600  $\text{cm}^{-1}$  region. All the spectra in Figure S1 consist of sharp bands with different vibronic patterns. The UV spectrum of bare  $\text{K}^+\cdot\text{DB18C6}$  (Figure S1a) has its band origin at 36 415  $\text{cm}^{-1}$ ,<sup>4</sup> which is 700  $\text{cm}^{-1}$  higher than that of jet-cooled neutral DB18C6 monomer.<sup>23</sup> The spectra of the hydrated complexes are also higher in energy than the DB18C6 monomer,<sup>23,24</sup> although to a lesser degree. The relative band positions of the

UV absorption of the  $\text{K}^+\cdot\text{DB18C6}\cdot(\text{H}_2\text{O})_n$  complexes reflect the strength of the intermolecular interaction between DB18C6 and the other components in the complexes. The UV spectra of the  $n = 1–4$  complexes increasingly shift to the red with increasing cluster size, which suggests a progressive decrease in the intermolecular interaction with DB18C6. For the  $n = 5$  complex, the vibronic bands shift to higher frequency again, followed by a gradual shift to lower frequency for complexes with  $n = 6–8$ . Another noticeable feature of this series of UVPD spectra is that the  $n = 4$  complex shows highly congested features compared to those of the other complexes.

Figure S2 of the Supporting Information shows the UVPD spectra of the  $\text{Rb}^+\cdot\text{DB18C6}\cdot(\text{H}_2\text{O})_n$  ( $n = 0–8$ ) complexes, which exhibit a similar trend as the corresponding potassiated species. The 0–0 band in the spectrum of  $\text{Rb}^+\cdot\text{DB18C6}$  (Figure S2a) appears at 36 319  $\text{cm}^{-1}$ ,<sup>4</sup> with those of the hydrated complexes progressively shifting to lower energy for  $n = 1–4$  before shifting to higher frequency again at  $n = 5$ . The UVPD spectrum of the  $n = 4$  complex (Figure S2e) shows congested features, similar to that of the  $\text{K}^+\cdot\text{DB18C6}\cdot(\text{H}_2\text{O})_4$  complex (Figure S1e). Unlike the case of the doubly hydrated potassiated species (Figure S1c), the  $\text{Rb}^+\cdot\text{DB18C6}\cdot(\text{H}_2\text{O})_2$  complex shows congested spectral features with no strong origin band (Figure S2c).

The UVPD spectra of the  $\text{Cs}^+\cdot\text{DB18C6}\cdot(\text{H}_2\text{O})_n$  ( $n = 0–8$ ) complexes are shown in Figure S3 of the Supporting Information. The origin band of  $\text{Cs}^+\cdot\text{DB18C6}$  appears at 36 234  $\text{cm}^{-1}$  (Figure S3a).<sup>4</sup> Similar to  $\text{K}^+$  and  $\text{Rb}^+$ , the UV bands of the  $\text{Cs}^+$  complexes shift to lower frequency with increasing hydration. However, one difference for the  $\text{Cs}^+$  spectra (Figure S3) from the  $\text{K}^+$  and  $\text{Rb}^+$  spectra (Figures S1 and S2) is that the UV bands continuously shift to lower frequency from  $n = 1$  to 5 before exhibiting a blue shift at  $n = 6$ . Moreover, in the case of the  $\text{Cs}^+$  complexes, it is the  $n = 5$  species (Figure S3f) that exhibits particularly congested vibronic features. In the spectra of the  $n = 2$  and 4 complexes (Figure S3c and e), a number of sharp bands appear much more closely than the case of  $\text{Rb}^+$ . These spectral features will represent the complex structure, which will be described in more detail in the following sections.

**3.2. Computed Structures.** Figure 1 shows optimized computed structures of the  $M^+\cdot\text{DB18C6}\cdot(\text{H}_2\text{O})_n$  ( $M = \text{K}, \text{Rb}, \text{Cs}; n = 1–5$ ) complexes obtained at the M05-2X/6-311++G(d,p) level. We have previously determined the structure of bare complexes (K-a, Rb-a, and Cs-b)<sup>4</sup> and have confirmed that the conformers of the hydrated  $\text{K}^+\cdot\text{DB18C6}$  complexes shown in Figure 1 exist in the experiment under cold gas-phase conditions.<sup>6</sup> For the hydrated  $\text{Rb}^+\cdot\text{DB18C6}$  and  $\text{Cs}^+\cdot\text{DB18C6}$  complexes, the most stable conformers (or the second most stable conformer for  $\text{Cs}^+\cdot\text{DB18C6}\cdot(\text{H}_2\text{O})_1$ ) are displayed in Figure 1. The most and the second most stable structures of the  $M^+\cdot\text{DB18C6}\cdot(\text{H}_2\text{O})_n$  complexes are shown with the total energy in Figures S4–S8 of the Supporting Information. All the complexes in Figure 1 have a boat-type form in the  $M^+\cdot\text{DB18C6}$  part. In all the isomers of the  $\text{Rb}^+\cdot\text{DB18C6}\cdot(\text{H}_2\text{O})_n$  and  $\text{Cs}^+\cdot\text{DB18C6}\cdot(\text{H}_2\text{O})_n$  complexes, the  $\text{H}_2\text{O}$  molecules are located only on top of a boat-type  $M^+\cdot\text{DB18C6}$  conformer, even for the complexes smaller than  $n = 4$ ; the  $\text{K}^+\cdot\text{DB18C6}\cdot(\text{H}_2\text{O})_{2,3}$  complexes have the  $\text{H}_2\text{O}$  molecules on both sides of the boat  $\text{K}^+\cdot\text{DB18C6}$  conformer (Figure 1). This is in strong contrast to the  $\text{K}^+\cdot\text{DB18C6}\cdot(\text{H}_2\text{O})_n$  ( $n = 1–3$ ) complexes, where the  $\text{H}_2\text{O}$  molecules are located either on top or bottom, or on both sides.<sup>6</sup> As will be demonstrated below, we propose

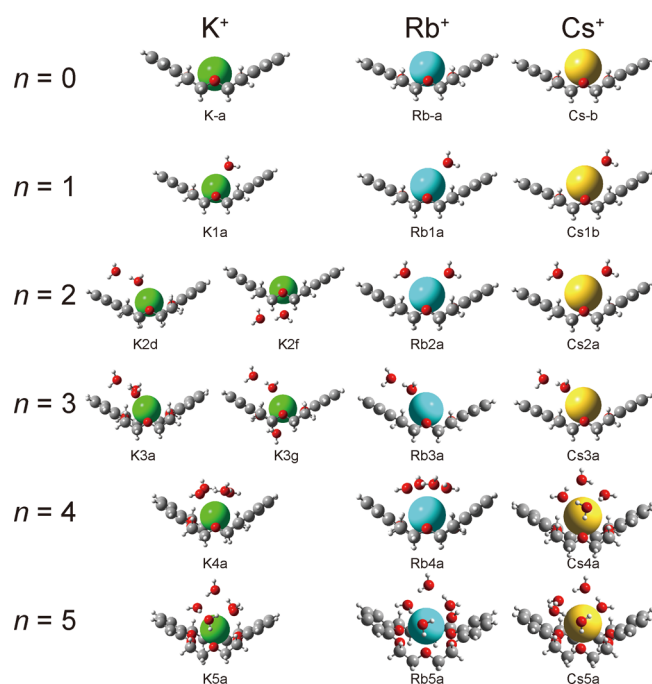


**Figure 1.** Optimized structures of the  $M^+\cdot\text{DB18C6}\cdot(\text{H}_2\text{O})_n$  ( $M = \text{K}, \text{Rb}, \text{Cs}; n = 0-5$ ) calculated at the M05-2X/6-311++G(d,p) level. The structures of bare complexes (K-a, Rb-a, and Cs-b) were determined in our gas-phase study (ref 4). It was confirmed in ref 6 that the conformers of the  $\text{K}^+\cdot\text{DB18C6}\cdot(\text{H}_2\text{O})_{1-5}$  complexes in this figure exist in the experiment under cold gas-phase conditions. For the hydrated  $\text{Rb}^+\cdot\text{DB18C6}$  and  $\text{Cs}^+\cdot\text{DB18C6}$  complexes, the most stable conformers (or the second most stable one for  $\text{Cs}^+\cdot\text{DB18C6}\cdot(\text{H}_2\text{O})_i$ ; see text) are displayed in this figure. Other optimized structures of the hydrated complexes are displayed with the relative total energy in the Supporting Information.

the structure of the hydrated complexes on the basis of UVPD and IR-UV spectra, not of the stability order of isomers in quantum chemical calculations. The calculated total energy of the conformers cannot be used as definitive evidence for the structural assignment of the complexes, because it highly depends on the calculation level.

**3.3. IR Spectra.** We have reported conformer-selective, IR-UV double-resonance spectra of the  $\text{K}^+\cdot\text{DB18C6}\cdot(\text{H}_2\text{O})_n$  ( $n = 1-5$ ) complexes in our previous study.<sup>6</sup> The smaller abundance of the hydrated  $\text{Rb}^+\cdot\text{DB18C6}$  and  $\text{Cs}^+\cdot\text{DB18C6}$  complexes prevented us from measuring exhaustive IR-UV spectra, but we have succeeded in obtaining spectra for some of them. Figure 2 shows the IR-UV (red curves) and theoretical IR (black curves and bars) spectra of the  $\text{Rb}^+\cdot\text{DB18C6}\cdot(\text{H}_2\text{O})_n$  ( $n = 1-3$ ) complexes in the OH stretching region. Black bars present calculated results of the oscillator strength and vibrational frequency, and black curves are produced by distributing a Lorentzian function with intensity proportional to the oscillator strength and a full width at half maximum (fwhm) of  $5\text{ cm}^{-1}$  to each vibration. The UV probe positions at which the IR-UV spectra are measured are shown with arrows in Figure S2 of the Supporting Information. The top curves in Figures 2a–c are the IR-UV gain spectra measured at nonresonant UV positions, which should reflect the IR spectra of all conformers present in the experiment. In the case of the  $n = 1$  complex (Figure 2a), the signal-to-noise ratio of the gain spectrum is not so high, but it gives two IR bands at  $3609$  and  $3712\text{ cm}^{-1}$ , which are highlighted by arrows. The calculated IR spectrum of isomer

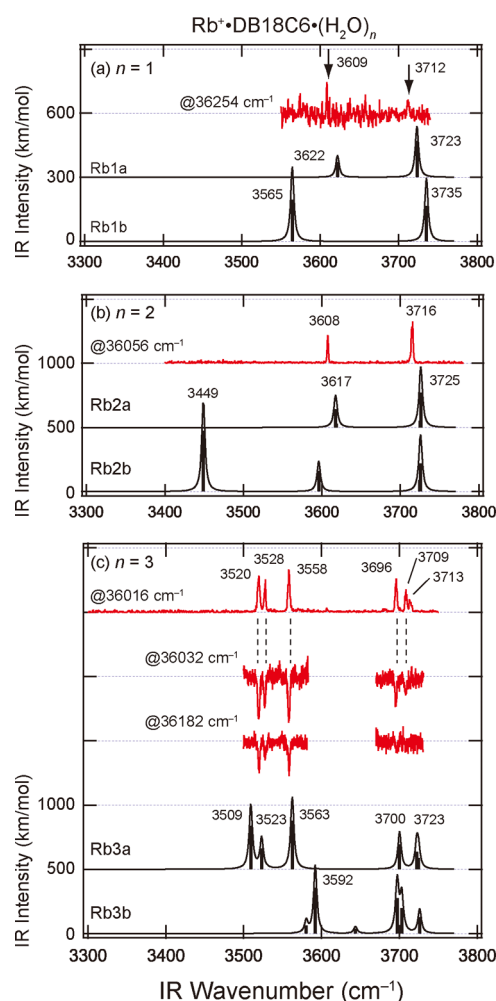


**Figure 2.** IR-UV (red curves) and theoretical IR (black curves and bars) spectra of the  $\text{Rb}^+\cdot\text{DB18C6}\cdot(\text{H}_2\text{O})_{1-3}$  complexes. The UV frequency at which the intensity of fragment ions is monitored for the IR-UV spectra is shown with the arrows in Figure S2 of the Supporting Information.

$\text{Rb1a}$  (Figure 1) well reproduces the obtained gain spectrum. The second most stable isomer ( $\text{Rb1b}$ , Figure S5 of the Supporting Information) has a characteristic IR band at  $3565\text{ cm}^{-1}$ . This band corresponds to the stretching vibration of the OH group hydrogen-bonded to an ether oxygen. In the IR-UV gain spectrum, no strong band is observed around  $3560\text{ cm}^{-1}$ , suggesting that isomer  $\text{Rb1b}$  is not present in the experiment.

For the  $n = 2$  complex, the IR-UV gain spectrum (top spectrum in Figure 2b) shows bands at  $3608$  and  $3716\text{ cm}^{-1}$ , but no band is found in the  $3400-3600\text{ cm}^{-1}$  region. This IR-UV gain spectrum is quite similar to the theoretical one of isomer  $\text{Rb2a}$  (Figure 1). The second most stable isomer ( $\text{Rb2b}$ , Figure S5 of the Supporting Information) is predicted to have a strong band at  $3449\text{ cm}^{-1}$  due to the stretching vibration of the hydrogen-bonded OH group. However, the IR-UV gain spectrum shows no such band, indicating the absence of isomer  $\text{Rb2b}$  in the experiment.

Infrared spectra of the  $\text{Rb}^+\cdot\text{DB18C6}\cdot(\text{H}_2\text{O})_3$  complex are shown in Figure 2c.<sup>6</sup> The IR-UV gain spectrum (top spectrum in Figure 2c) shows peaks at  $3520$ ,  $3528$ ,  $3558$ ,  $3696$ , and  $3709\text{ cm}^{-1}$ , accompanied by a weak shoulder at  $3713\text{ cm}^{-1}$ . We measure IR-UV dip spectra at two resonant UV positions ( $36032$  and  $36182\text{ cm}^{-1}$ ). The IR-UV depletion spectrum



measured at  $36\,032\text{ cm}^{-1}$  clearly shows five dips at the same positions with those of the gain spectrum. This indicates that the IR-UV bands of the  $n = 3$  complex are due to a single isomer. The depth is not high, but the IR-UV spectrum at  $36\,182\text{ cm}^{-1}$  is similar to that measured at  $36\,032\text{ cm}^{-1}$ , confirming the presence of a single conformer. The spectral pattern of the theoretical IR spectrum of isomer Rb3a (Figure 1) well reproduces the observed IR-UV spectra, exhibiting three bands around  $3500\text{ cm}^{-1}$  and two bands around  $3700\text{ cm}^{-1}$ . In contrast, the spectral features of the second most stable isomer (Rb3b, Figure S5 of the Supporting Information) are sufficiently different from those of the measured spectra. From these results, the IR-UV spectra of the  $n = 1$ – $3$  complexes can be described by theoretical IR spectra of the most stable isomers (Rb1a, Rb2a, and Rb3a).

Figure 3 displays the IR-UV (red curves) and theoretical IR (black curves and bars) spectra of the  $\text{Rb}^+\cdot\text{DB18C6}\cdot(\text{H}_2\text{O})_{4,5}$

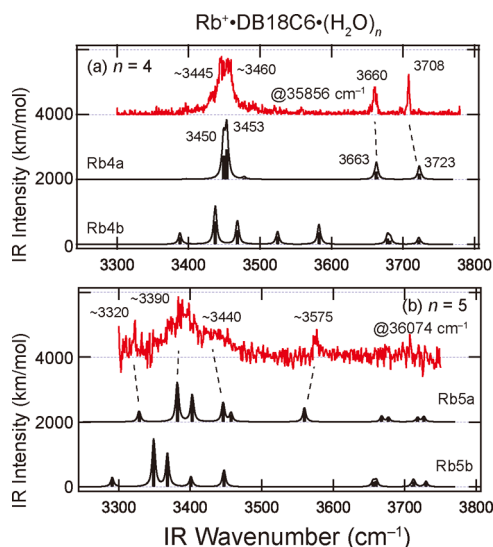


**Figure 3.** IR-UV (red curves) and theoretical IR (black curves and bars) spectra of the  $\text{Rb}^+\cdot\text{DB18C6}\cdot(\text{H}_2\text{O})_{4,5}$  complexes. The UV frequency at which the intensity of fragment ions is monitored for the IR-UV spectra is shown with the arrows in Figure S2 of the Supporting Information.

complexes. In the IR-UV gain spectrum of the  $n = 4$  complex (top spectrum of Figure 3a), peaks are seen at  $\sim 3445$ ,  $\sim 3460$ ,  $3660$ , and  $3708\text{ cm}^{-1}$ . The most stable isomer of the  $n = 4$  complex (Rb4a, Figure 1) reproduces the IR spectrum with peaks at  $3450$ ,  $3453$ ,  $3663$ , and  $3723\text{ cm}^{-1}$ . The IR-UV gain spectrum of the  $n = 5$  complex (Figure 3b) has broad absorption in the  $3300$ – $3500\text{ cm}^{-1}$  region and a weak one at  $\sim 3575\text{ cm}^{-1}$ . These spectral patterns are reasonably well reproduced by the calculated IR spectrum of isomer Rb5a (Figure 1).

Figure 4 presents the IR-UV (red curves) and theoretical IR (black curves and bars) spectra of the  $\text{Cs}^+\cdot\text{DB18C6}\cdot(\text{H}_2\text{O})_3$  complex, reproduced from our previous paper.<sup>6</sup> The IR-UV gain and dip spectra (top two spectra of Figure 4) are similar to each other; IR bands are found at  $3511$ ,  $3524$ ,  $3553$ ,  $3694$ , and  $3705\text{ cm}^{-1}$ . Therefore, the IR-UV gain spectrum of the  $\text{Cs}^+\cdot\text{DB18C6}\cdot(\text{H}_2\text{O})_3$  complex is attributed to a single isomer. The spectral patterns of the IR-UV spectra of the  $\text{Cs}^+\cdot\text{DB18C6}\cdot(\text{H}_2\text{O})_3$  complex resemble those of the  $\text{Rb}^+\cdot\text{DB18C6}\cdot(\text{H}_2\text{O})_3$  complex (Figure 2c). In addition, the most stable calculated

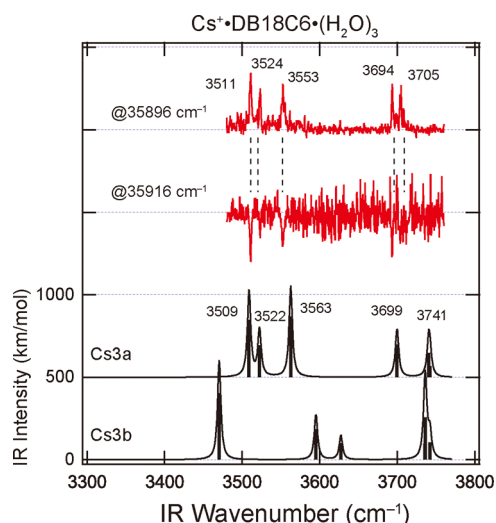


**Figure 4.** IR-UV (red curves) and theoretical IR (black curves and bars) spectra of the  $\text{Cs}^+\cdot\text{DB18C6}\cdot(\text{H}_2\text{O})_3$  complexes. The UV frequency at which the intensity of fragment ions is monitored for the IR-UV spectra is shown with the arrows in Figure S3 of the Supporting Information.

isomer (Cs3a, Figure 1) shows an IR spectrum similar to that we measure. In the following section, we discuss the probable structure of the  $\text{M}^+\cdot\text{DB18C6}\cdot(\text{H}_2\text{O})_n$  complexes on the basis of the UVPD, IR-UV, and theoretical results described above.

## 4. DISCUSSION

**4.1.  $\text{M}^+\cdot\text{DB18C6}\cdot(\text{H}_2\text{O})_1$  Complexes.** In our previous work, we determined the hydration structure of the  $\text{K}^+\cdot\text{DB18C6}\cdot(\text{H}_2\text{O})_{1-5}$  complexes by IR spectroscopy in the OH stretching region.<sup>6</sup> Here we determine structure of the hydrated  $\text{Rb}^+\cdot\text{DB18C6}$  and  $\text{Cs}^+\cdot\text{DB18C6}$  complexes using a combination of UVPD and IR spectra. Figure 5 displays the UVPD spectra of the  $\text{M}^+\cdot\text{DB18C6}\cdot(\text{H}_2\text{O})_1$  ( $\text{M} = \text{K}, \text{Rb}, \text{and Cs}$ ) complexes for comparison. For the  $\text{K}^+\cdot\text{DB18C6}\cdot(\text{H}_2\text{O})_1$  complex, all the bands are attributed to a single isomer (K1a, Figure 1).<sup>6</sup> In this isomer, the oxygen atom of the  $\text{H}_2\text{O}$  molecule is directly attached to the  $\text{K}^+$  ion, and one of the OH groups forms the  $\text{O}-\text{H}\cdots\pi$  hydrogen bond with one of the benzene rings. As a result, the two benzene rings are not equivalent. Time-dependent density functional theory (TD-DFT) calculations of the  $\text{K}^+\cdot\text{DB18C6}\cdot(\text{H}_2\text{O})_1$  complex predicts that the  $\text{S}_1-\text{S}_0$  and  $\text{S}_2-\text{S}_0$  transition energies of isomer K1a differ by  $>100\text{ cm}^{-1}$ , and the  $\text{S}_1-\text{S}_0$  transition is localized almost entirely on the benzene ring involved in the  $\text{O}-\text{H}\cdots\pi$  hydrogen bond. In addition, the vibronic structures starting from  $36\,274$  and  $36\,334\text{ cm}^{-1}$  show different features from each other (an expanded view of the UVPD spectrum is shown in Figure S11 of the Supporting Information). On the basis of these theoretical and experimental results, the two strong bands observed at  $36\,274$  and  $36\,334\text{ cm}^{-1}$  (Figure 5a) can be reasonably assigned to the  $0-0$  band of the  $\text{S}_1-\text{S}_0$  and  $\text{S}_2-\text{S}_0$  transitions.

The structure of the  $\text{Rb}^+\cdot\text{DB18C6}\cdot(\text{H}_2\text{O})_1$  complex should be similar to that of the  $\text{K}^+\cdot\text{DB18C6}\cdot(\text{H}_2\text{O})_1$  complex, because the IR-UV spectrum of the former (Figure 2a) in the region of the OH stretching bands strongly resembles that of the latter (Figure 2a of ref 6). Moreover, isomer Rb1a of the  $\text{Rb}^+$  complex (Figure 1) has a structure similar to that of the  $\text{K}^+$  complex determined in our previous paper (K1a, Figure 1).<sup>6</sup>

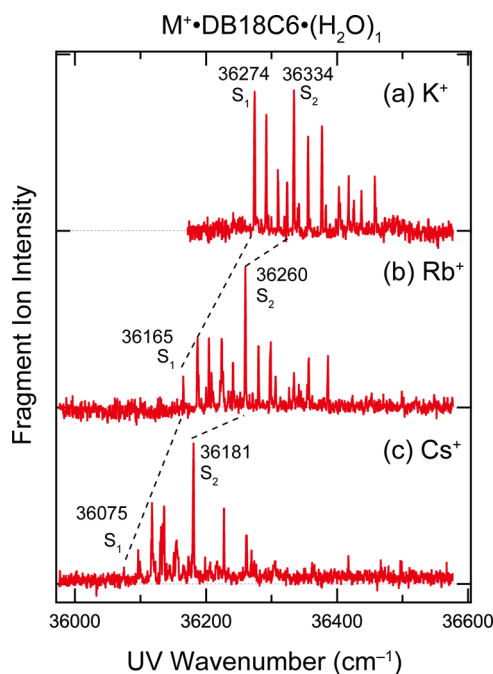


**Figure 5.** UVPD spectra of the  $M^+\cdot\text{DB18C6}\cdot(\text{H}_2\text{O})_1$  ( $M = \text{K}, \text{Rb},$  and  $\text{Cs}$ ) complexes. The intensity of each spectrum is normalized as having the same maximum intensity for all the spectra. The spectrum of the  $\text{K}^+$  complex (a) was taken from ref 6.

We thus assign the structure of isomer Rb1a in Figure 1 to the  $\text{Rb}^+\cdot\text{DB18C6}\cdot(\text{H}_2\text{O})_1$  complex. We also suppose that the strong sharp band observed at  $36\,260\text{ cm}^{-1}$  in the UVPD spectrum of  $\text{Rb}^+\cdot\text{DB18C6}\cdot(\text{H}_2\text{O})_1$  (Figure 5b) is the 0–0 band of the  $\text{S}_2\text{--S}_0$  transition, which would make the weak band at  $36\,165\text{ cm}^{-1}$  the 0–0 band of the  $\text{S}_1\text{--S}_0$  transition. As mentioned above, the  $\text{S}_1\text{--S}_0$  transition of the  $\text{K}^+\cdot\text{DB18C6}\cdot(\text{H}_2\text{O})_1$  complex is mainly localized in the benzene ring having the  $\text{O--H}\cdots\pi$  hydrogen bond, and a similar localization can be seen also in the calculation of  $\text{Rb}^+\cdot\text{DB18C6}\cdot(\text{H}_2\text{O})_1$ .

While an IR spectrum is not available for the  $\text{Cs}^+\cdot\text{DB18C6}\cdot(\text{H}_2\text{O})_1$  complex, it is possible to infer the structure on the basis of the UVPD spectrum. As shown in Figure 5c, the UVPD spectrum of the  $\text{Cs}^+\cdot\text{DB18C6}\cdot(\text{H}_2\text{O})_1$  complex is quite similar to that of the corresponding  $\text{Rb}^+$  complex. A strong, sharp band is observed at  $36\,181\text{ cm}^{-1}$ , which can be attributed to the 0–0 band of the  $\text{S}_2\text{--S}_0$  transition, and we assign the weak band at  $36\,075\text{ cm}^{-1}$  to the 0–0 band of the  $\text{S}_1\text{--S}_0$  transition. The amount of the red-shift from  $\text{Rb}^+\cdot\text{DB18C6}\cdot(\text{H}_2\text{O})^+$  to  $\text{Cs}^+\cdot\text{DB18C6}\cdot(\text{H}_2\text{O})$  is  $\sim 85\text{ cm}^{-1}$ , which is comparable to that between unsolvated  $\text{Rb}^+\cdot\text{DB18C6}$  and  $\text{Cs}^+\cdot\text{DB18C6}$  ( $85\text{ cm}^{-1}$ ).<sup>4</sup> The similarity of this spectrum to that of the  $\text{Rb}^+$  complex indicates a similar structure. The two most stable isomers of the  $\text{Cs}^+\cdot\text{DB18C6}\cdot(\text{H}_2\text{O})_1$  complex are shown in Figure S7 of the Supporting Information. Among them, isomer Cs1b (Figure 1) has a structure similar to that of  $\text{Rb}^+\cdot\text{DB18C6}\cdot(\text{H}_2\text{O})_1$  (Rb1a, Figure 1). Hence, we assign the structure of  $\text{Cs}^+\cdot\text{DB18C6}\cdot(\text{H}_2\text{O})_1$  to isomer Cs1b. Isomer Cs1b (Figure 1) is the second most stable structure of the  $\text{Cs}^+\cdot\text{DB18C6}\cdot(\text{H}_2\text{O})_1$  complex at the M05-2X/6-311++G(d,p) level. The DB18C6 has a boat-type open conformation, while in the most stable structure, Cs1a (Figure S7), a part of the DB18C6 ring is bent. Similar conformers (Cs-a and Cs-b) were also found in quantum chemical calculations of bare  $\text{Cs}^+\cdot\text{DB18C6}$ ,<sup>4</sup> which we determined to adopt the boat-type  $\text{C}_{2v}$  conformer (Cs-b) on

the basis of the UV spectrum; Cs-b well reproduces the position of the 0–0 band in the UVPD spectrum, and Cs-a has a transition energy  $>500\text{ cm}^{-1}$  higher than that of Cs-b.<sup>4</sup> Because the UV absorption of the  $\text{Cs}^+\cdot\text{DB18C6}\cdot(\text{H}_2\text{O})_n$  complexes shifts to lower frequency from  $n = 0$  to 1 (Figures S3a and b), the  $\text{Cs}^+\cdot\text{DB18C6}$  part in the  $\text{Cs}^+\cdot\text{DB18C6}\cdot(\text{H}_2\text{O})_1$  complexes should have a boat-type conformation similar to the structure of bare  $\text{Cs}^+\cdot\text{DB18C6}$  (Cs-b). Thus, isomer Cs1b is the most likely form for the  $\text{Cs}^+\cdot\text{DB18C6}\cdot(\text{H}_2\text{O})_1$  complex. Here it should be emphasized again that the structural assignment for the  $n = 1$  complexes described earlier is performed on the basis of the experimental UV and IR spectra, not of the calculated total energy of the isomers; isomers K1a and Rb1a (Figure 1), which are determined to be present in the experiment, are the most stable for the  $\text{K}^+\cdot\text{DB18C6}\cdot(\text{H}_2\text{O})_1$  and  $\text{Rb}^+\cdot\text{DB18C6}\cdot(\text{H}_2\text{O})_1$  complexes at the M05-2X/6-311++G(d,p) level, although the stability order of the isomers may be changed at different calculation levels.

**4.2.  $M^+\cdot\text{DB18C6}\cdot(\text{H}_2\text{O})_2$  Complexes.** The UVPD spectra of the  $M^+\cdot\text{DB18C6}\cdot(\text{H}_2\text{O})_2$  ( $M = \text{K}, \text{Rb},$  and  $\text{Cs}$ ) complexes are compared in Figure 6. The spectral patterns are quite different

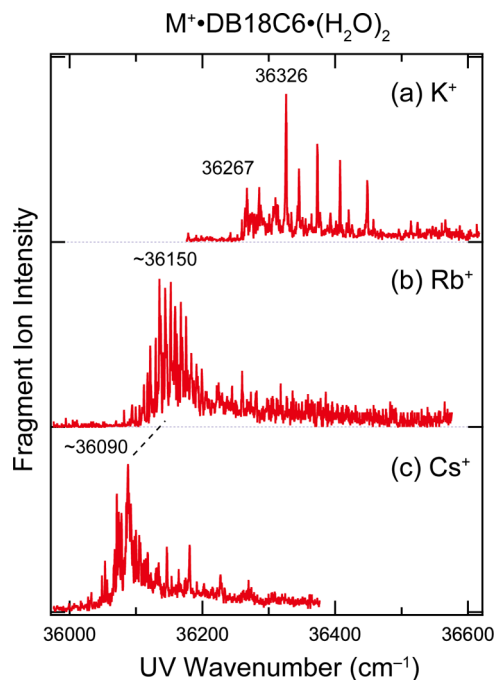


**Figure 6.** UVPD spectra of the  $M^+\cdot\text{DB18C6}\cdot(\text{H}_2\text{O})_2$  ( $M = \text{K}, \text{Rb},$  and  $\text{Cs}$ ) complexes. The intensity of each spectrum is normalized as having the same maximum intensity for all the spectra. The spectrum of the  $\text{K}^+$  complex (a) was taken from ref 6.

between the  $\text{K}^+$  and  $\text{Rb}^+$  complexes. The UVPD spectrum of the  $\text{K}^+\cdot\text{DB18C6}\cdot(\text{H}_2\text{O})_2$  complex (Figure 6a) appears relatively simple, with two sharp origin bands at  $36\,267$  and  $36\,326\text{ cm}^{-1}$ . In contrast, the UVPD spectrum of the  $\text{Rb}^+\cdot\text{DB18C6}\cdot(\text{H}_2\text{O})_2$  complex (Figure 6b) exhibits a congested progression with many sharp bands. The qualitative difference in the UVPD spectra of the  $\text{K}^+$  and  $\text{Rb}^+$  complexes suggest that they have substantially different structures. On the basis of previously measured IR-UV spectra of the  $\text{K}^+$  complex,<sup>6</sup> the UVPD bands at  $36\,267$  and  $36\,326\text{ cm}^{-1}$  have been assigned to two different isomers (K2f and K2d, respectively, Figure 1). These spectra show a strong IR band at  $\sim 3453\text{ cm}^{-1}$ , which is assigned to the

stretching vibration of the OH group hydrogen-bonded to the other H<sub>2</sub>O molecule.<sup>6</sup> These two H<sub>2</sub>O molecules are bound on top or on the bottom of the boat-type K<sup>+</sup>·DB18C6 conformer. In contrast, the IR-UV gain spectrum of the Rb<sup>+</sup>·DB18C6·(H<sub>2</sub>O)<sub>2</sub> complex, shown in Figure 2b, does not exhibit a band around 3450 cm<sup>-1</sup>; the IR band positions of the Rb<sup>+</sup>·DB18C6·(H<sub>2</sub>O)<sub>2</sub> complex (3608 and 3716 cm<sup>-1</sup>) are almost the same as that of Rb<sup>+</sup>·DB18C6·(H<sub>2</sub>O)<sub>1</sub> (3609 and 3712 cm<sup>-1</sup>, Figure 2a). Hence, the two H<sub>2</sub>O molecules in the Rb<sup>+</sup>·DB18C6·(H<sub>2</sub>O)<sub>2</sub> complex appear to be bound independently to the Rb<sup>+</sup>·DB18C6 in a manner similar to that in the Rb<sup>+</sup>·DB18C6·(H<sub>2</sub>O)<sub>1</sub> complex. As seen in Figure 1, isomer Rb2a of the Rb<sup>+</sup>·DB18C6·(H<sub>2</sub>O)<sub>2</sub> complex has a hydration structure similar to that of Rb<sup>+</sup>·DB18C6·(H<sub>2</sub>O)<sub>1</sub> (Rb1a, Figure 1). The calculated IR spectrum of isomer Rb2a well reproduces the band position of the measured spectrum (Figure 2b). We conclude that the Rb<sup>+</sup>·DB18C6·(H<sub>2</sub>O)<sub>2</sub> complex has the structure of isomer Rb2a in Figure 1. The two benzene rings in this isomer are equivalent, leading to a complex with C<sub>2</sub> symmetry. This may enhance the exciton coupling between the two benzene rings leading to congested spectral features, as seen for the bare M<sup>+</sup>·DB18C6 (M = K, Rb, and Cs) complexes and for K<sup>+</sup>·DB18C6·(H<sub>2</sub>O)<sub>4</sub>.<sup>4,6</sup>

We consider now the structure of the Cs<sup>+</sup>·DB18C6·(H<sub>2</sub>O)<sub>2</sub> complex on the basis of the UVPD spectrum and the theoretical calculations. The UVPD spectrum of Cs<sup>+</sup>·DB18C6·(H<sub>2</sub>O)<sub>2</sub> (Figure 6c) more closely resembles that of Rb<sup>+</sup>·DB18C6·(H<sub>2</sub>O)<sub>2</sub> complex rather than that of K<sup>+</sup>·DB18C6·(H<sub>2</sub>O)<sub>2</sub>, with many sharp, closely spaced bands. Isomer Cs2a of Cs<sup>+</sup>·DB18C6·(H<sub>2</sub>O)<sub>2</sub> (Figure 1) has a structure similar to that of the Rb<sup>+</sup>·DB18C6·(H<sub>2</sub>O)<sub>2</sub> complex (Rb2a, Figure 1). Hence, we tentatively ascribe the structure of Cs<sup>+</sup>·DB18C6·(H<sub>2</sub>O)<sub>2</sub> to isomer Cs2a; definitive assignment with IR-UV spectroscopy, which includes further improvement of detection efficiency of the photodissociation spectrometer, is our future work.

**4.3. M<sup>+</sup>·DB18C6·(H<sub>2</sub>O)<sub>3</sub> Complexes.** Figure 7 displays UVPD spectra of the M<sup>+</sup>·DB18C6·(H<sub>2</sub>O)<sub>3</sub> (M = K, Rb, and Cs) complexes. In contrast to the spectra of the *n* = 2 complexes (Figure 6), the spectral features of the *n* = 3 species are similar among the different cations (i.e., K<sup>+</sup>, Rb<sup>+</sup>, and Cs<sup>+</sup>). The spectra are not as congested as that of Rb<sup>+</sup>·DB18C6·(H<sub>2</sub>O)<sub>2</sub> and Cs<sup>+</sup>·DB18C6·(H<sub>2</sub>O)<sub>2</sub>, and the vibronic structure starts with a strong band assignable to the 0–0 transition. The similarity of the UVPD spectra in Figure 7 suggests a similarity of the structures for the K<sup>+</sup>, Rb<sup>+</sup>, and Cs<sup>+</sup> complexes. In the case of K<sup>+</sup>·DB18C6·(H<sub>2</sub>O)<sub>3</sub>, two strong UV bands are found at 36 108 and 36 223 cm<sup>-1</sup> (Figure 7a). On the basis of the IR-UV experiments, these UV bands are assigned to the same isomer (K3a, Figure 1),<sup>6</sup> in which all three H<sub>2</sub>O molecules are located on top of the boat-type K<sup>+</sup>·DB18C6 conformer. Two of the H<sub>2</sub>O molecules are directly bound to the K<sup>+</sup> ion, and the third accepts hydrogen bonds from the other two, while donating an O–H···π hydrogen bond to one of the benzene rings. The two benzene rings in K3a are not equivalent; TD-DFT calculations show that the S<sub>1</sub>–S<sub>0</sub> and S<sub>2</sub>–S<sub>0</sub> electronic transitions of K3a are localized in either of the benzene rings and appear at different UV frequencies. In addition, the vibronic structures starting from 36 108 and 36 223 cm<sup>-1</sup> show different features from each other. Hence, the bands at 36 108 and 36 223 cm<sup>-1</sup> can be assigned to the 0–0 band of the S<sub>1</sub>–S<sub>0</sub> and S<sub>2</sub>–S<sub>0</sub> transitions of isomer K3a, respectively. Isomers Rb3a and Cs3a of the Rb<sup>+</sup> and Cs<sup>+</sup> complexes (Figure 1) resemble isomer K3a, and their IR-UV spectra (red curves in Figures 2c and 4) are similar to

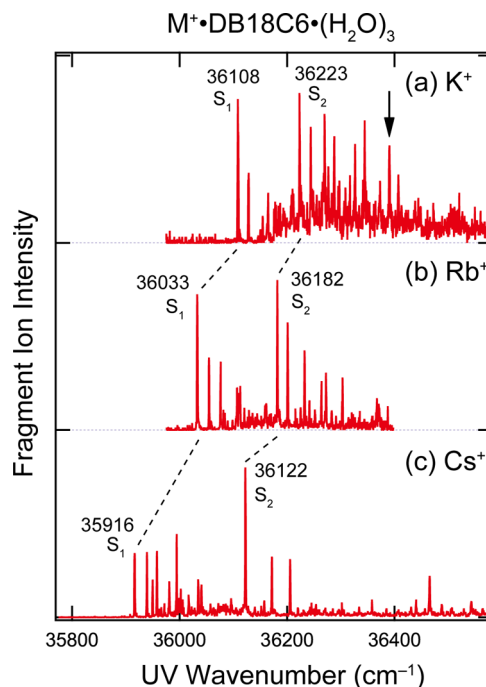


**Figure 7.** UVPD spectra of the M<sup>+</sup>·DB18C6·(H<sub>2</sub>O)<sub>3</sub> (M = K, Rb, and Cs) complexes. The intensity of each spectrum is normalized as having the same maximum intensity for all the spectra. The spectrum of the K<sup>+</sup> complex (a) was taken from ref 6. A sharp band highlighted with an arrow in (a) is assigned to an isomer other than that showing the strong bands at 36 108 and 36 223 cm<sup>-1</sup> (ref 6).

those of the K<sup>+</sup> complex (Figure 5b of ref 6). Moreover, the calculated IR spectra of Rb3a and Cs3a well reproduce the measured IR-UV spectra of the Rb<sup>+</sup>·DB18C6·(H<sub>2</sub>O)<sub>3</sub> and Cs<sup>+</sup>·DB18C6·(H<sub>2</sub>O)<sub>3</sub> complexes (Figures 2c and 4, respectively). Hence, we attribute the structure of the Rb<sup>+</sup>·DB18C6·(H<sub>2</sub>O)<sub>3</sub> and Cs<sup>+</sup>·DB18C6·(H<sub>2</sub>O)<sub>3</sub> complexes to isomers Rb3a and Cs3a, respectively (Figure 1). The strong bands observed at 36 033 and 36 182 cm<sup>-1</sup> for Rb<sup>+</sup> (Figure 7b) and at 35 916 and 36 122 cm<sup>-1</sup> for Cs<sup>+</sup> (Figure 7c) are assigned to the origin band of the S<sub>1</sub>–S<sub>0</sub> and S<sub>2</sub>–S<sub>0</sub> transitions. In the case of the K<sup>+</sup>·DB18C6·(H<sub>2</sub>O)<sub>3</sub> complex, there appears to be another isomer,<sup>6</sup> which exhibits a sharp UVPD band at 36 390 cm<sup>-1</sup> (highlighted by an arrow in Figure 7a). The structure of this isomer was determined to be isomer K3g (Figure 1) on the basis of its IR spectrum.<sup>6</sup> In this isomer, two H<sub>2</sub>O molecules are bound on top of the boat-type K<sup>+</sup>·DB18C6, and the other is bound on the bottom. This isomer shows a strong IR-UV band at 3463 cm<sup>-1</sup>, which does not seem to have an equivalent in the IR-UV spectrum of the Rb<sup>+</sup>·DB18C6·(H<sub>2</sub>O)<sub>3</sub> complex (top panel of Figure 2c). We conclude that the Rb<sup>+</sup> complex does not have an isomer analogous to K3g of the K<sup>+</sup> complex.

**4.4. M<sup>+</sup>·DB18C6·(H<sub>2</sub>O)<sub>n</sub> (*n* = 4–8) Complexes.** Figure 8 shows the UVPD spectra of the M<sup>+</sup>·DB18C6·(H<sub>2</sub>O)<sub>4</sub> (M = K, Rb, and Cs) complexes. The spectra of the K<sup>+</sup> and Rb<sup>+</sup> complexes (Figure 8a and b) both exhibit congested features with a number of sharp bands, suggesting a similarity of structure. In the previous study, the structure of the K<sup>+</sup>·DB18C6·(H<sub>2</sub>O)<sub>4</sub> complex was determined to be an isomer in which a ring of four H<sub>2</sub>O molecules is bound on top of the boat-type K<sup>+</sup>·DB18C6 (K4a in Figure 1).<sup>6</sup> Isomer Rb4a of the Rb<sup>+</sup> complex (Figure 1) has a structure similar to that of K4a, and its calculated IR spectrum well reproduces the IR-UV



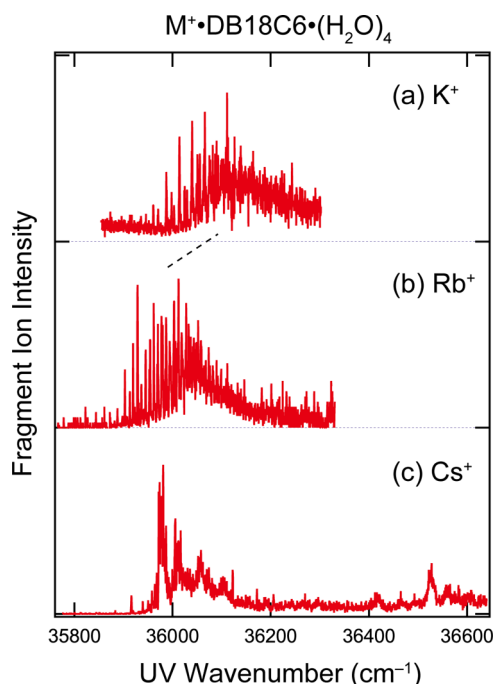


**Figure 8.** UVPD spectra of the  $M^+\cdot\text{DB18C6}\cdot(\text{H}_2\text{O})_4$  ( $M = \text{K}, \text{Rb},$  and  $\text{Cs}$ ) complexes. The intensity of each spectrum is normalized as having the same maximum intensity for all the spectra. The spectrum of the  $\text{K}^+$  complex (a) was taken from ref 6.

spectrum of the  $\text{Rb}^+$  complex (Figure 3a). Hence, the  $\text{Rb}^+\cdot\text{DB18C6}\cdot(\text{H}_2\text{O})_4$  complex is likely to have the structure of isomer  $\text{Rb4a}$ .

Figure 9 displays the UVPD spectra of the  $M^+\cdot\text{DB18C6}\cdot(\text{H}_2\text{O})_5$  ( $M = \text{K}, \text{Rb},$  and  $\text{Cs}$ ) complexes. The spectra of the  $\text{K}^+$

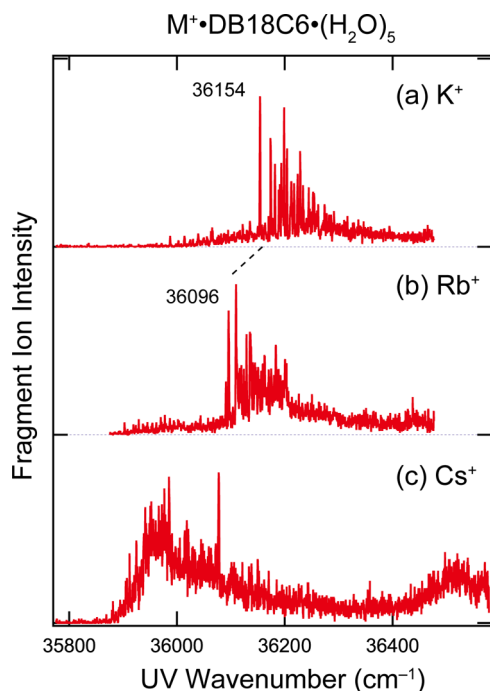


**Figure 9.** UVPD spectra of the  $M^+\cdot\text{DB18C6}\cdot(\text{H}_2\text{O})_5$  ( $M = \text{K}, \text{Rb},$  and  $\text{Cs}$ ) complexes. The intensity of each spectrum is normalized as having the same maximum intensity for all the spectra. The spectrum of the  $\text{K}^+$  complex (a) was taken from ref 6.

and  $\text{Rb}^+$  complexes each have a strong band assignable to the 0–0 transition, at 36 154 and 36 096  $\text{cm}^{-1}$ , respectively, and the similarity of the UVPD spectra suggests a similarity of their structures. In our previous study, the structure of the  $\text{K}^+\cdot\text{DB18C6}\cdot(\text{H}_2\text{O})_5$  complex was determined to be  $\text{K5a}$  (Figure 1).<sup>6</sup> Given that isomer  $\text{Rb5a}$  of the  $\text{Rb}^+$  complex (Figure 1) is similar to  $\text{K5a}$ , and the calculated IR spectrum of this isomer reproduces the IR-UV spectrum of the  $\text{Rb}^+\cdot\text{DB18C6}\cdot(\text{H}_2\text{O})_5$  complex (Figure 3b), we attribute its structure to isomer  $\text{Rb5a}$ .

In contrast to the case of the  $\text{Rb}^+$  complexes, the UV spectral features of  $\text{Cs}^+\cdot\text{DB18C6}\cdot(\text{H}_2\text{O})_{4,5}$  are substantially different from those of the  $\text{K}^+$  complexes (Figures 8 and 9). The UVPD spectrum of  $\text{Cs}^+\cdot\text{DB18C6}\cdot(\text{H}_2\text{O})_4$  (Figure 8c) does not show extensive vibrational progressions as do the corresponding  $\text{K}^+$  and  $\text{Rb}^+$  complexes. In the case of  $\text{Cs}^+\cdot\text{DB18C6}\cdot(\text{H}_2\text{O})_5$ , the UVPD spectrum (Figure 9c) seems to consist of a number of broad bands, whereas the corresponding  $\text{K}^+$  and  $\text{Rb}^+$  species show much simpler features with a strong 0–0 band. Because we do not have IR spectra of the  $\text{Cs}^+\cdot\text{DB18C6}\cdot(\text{H}_2\text{O})_{4,5}$  complexes, it is difficult to determine their structure definitely. However, as seen in Figure 1, the optimized structures of the  $\text{Cs}^+\cdot\text{DB18C6}\cdot(\text{H}_2\text{O})_{4,5}$  complexes (Figures 1, S7, and S8) have a structure different from those of the  $\text{K}^+$  ( $\text{K4a}$  and  $\text{K5a}$ ) and  $\text{Rb}^+$  ( $\text{Rb4a}$  and  $\text{Rb5a}$ ) species. In isomer  $\text{Cs4a}$ , the four-membered ring of the  $\text{H}_2\text{O}$  molecules is hydrogen-bonded to one of the oxygen atoms in the  $\text{DB18C6}$  part, while in isomers  $\text{K4a}$  and  $\text{Rb4a}$  the four-membered ring is bound right on top of the metal ion, apart from the crown cavity. The difference in the structure between  $\text{Cs5a}$  and  $\text{K5a}$  or  $\text{Rb5a}$  is not so obvious; in all of these isomers, a five-membered  $\text{H}_2\text{O}$  ring is bound to the metal ions. However, because the radius of the  $\text{Cs}^+$  ion is larger than that of  $\text{K}^+$  and  $\text{Rb}^+$ , the position of the  $\text{H}_2\text{O}$  ring relative to the  $M^+\cdot\text{DB18C6}$  component in isomer  $\text{Cs5a}$  is substantially different from that in  $\text{K5a}$  and  $\text{Rb5a}$ . These calculations of the  $\text{Cs}^+$  complexes are consistent with the UVPD spectra in Figures 8 and 9. We thus tentatively suggest that the  $\text{Cs}^+\cdot\text{DB18C6}\cdot(\text{H}_2\text{O})_{4,5}$  complexes can have a structure like  $\text{Cs4a}$  and  $\text{Cs5a}$ , respectively. It should be noted that this is a tentative assignment for the  $n = 4$  and 5 complexes of  $\text{Cs}^+$  on the basis of the geometry optimization calculated at the  $\text{M05-2X/6-311++G(d,p)}$  level. Definitive determination of the structure by IR-UV spectroscopy and higher-level calculations is our future work.

The UVPD spectra of the  $M^+\cdot\text{DB18C6}\cdot(\text{H}_2\text{O})_{6-8}$  ( $M = \text{K}, \text{Rb},$  and  $\text{Cs}$ ) complexes are shown in Figures S1–3 of the Supporting Information. Because the attachment of the metal ions to bare  $\text{DB18C6}$  shifts the UV absorption to the blue, the UV band position or the amount of the blue shift can represent a strength scale of the intermolecular interaction that the  $\text{DB18C6}$  part has in the  $M^+\cdot\text{DB18C6}\cdot(\text{H}_2\text{O})_n$  complexes.<sup>4</sup> One of the overall trends in the UV spectra of the complexes investigated in this work is that the band position gradually shifts to the red with increasing numbers of water molecules, which indicates that the interaction that the  $\text{DB18C6}$  part has becomes weaker and weaker with increasing hydration number but then at some point shifts back to the blue before continuing to red-shift at still higher hydration. This jump back to higher energy occurs between  $n = 4$  and 5 for the  $\text{K}^+$  and  $\text{Rb}^+$  complexes and between  $n = 5$  and 6 for the  $\text{Cs}^+$  complexes. This trend in the UVPD spectra is related to the hydration manner in hydrated alkali metal ions,  $M^+\cdot(\text{H}_2\text{O})_n$ . Miller and Lisy reported the structure of hydrated alkali metal ions determined by IR spectroscopy in the gas phase.<sup>25,26</sup> They

found that the  $K^+ \cdot (H_2O)_4$  complex has a four-membered  $H_2O$  ring, indicating that this ring size is suitable for effective hydration to  $K^+$  ion. In the case of the  $K^+ \cdot (H_2O)_5$  complex, four water molecules form a ring through four  $O-H \cdots O$  hydrogen bonds, and this ring is bound to the  $K^+$  ion. The other  $H_2O$  molecule is bound to the  $K^+$  ion on the opposite side of the  $H_2O$  ring.<sup>25,26</sup> This result suggests that, in binding to the  $K^+$  ion, a ring with four  $H_2O$  molecules is preferred over a ring with five  $H_2O$  molecules. For the  $K^+ \cdot DB18C6 \cdot (H_2O)_n$  ( $n = 4$  and  $5$ ) complexes, all the  $H_2O$  molecules are bound on top of the  $K^+ \cdot DB18C6$  part, forming a ring (Figure 1); the  $K^+$  ion is located between the  $H_2O$  ring and the  $DB18C6$  component. The binding ability of  $H_2O$  rings to the  $K^+$  ion seems to affect in turn the interaction between the  $DB18C6$  part and  $K^+$  in these complexes. In the  $K^+ \cdot DB18C6 \cdot (H_2O)_4$  complex (K4a in Figure 1), the four-membered  $H_2O$  ring attracts strongly the  $K^+$  ion, which can weaken the interaction between the  $K^+$  ion and the  $DB18C6$  part and provide the least blue-shifted UV absorption of  $DB18C6$  among the  $n = 0-8$  complexes (Figure S1). As expected from the hydration manner in  $K^+ \cdot (H_2O)_5$ , the binding strength of the five-membered  $H_2O$  ring to the  $K^+$  ion is smaller than that of the four-membered species. Weaker interaction of the  $K^+$  ion with the five-membered  $H_2O$  ring results in stronger interaction with the  $DB18C6$  part, showing the blue-shift of the  $DB18C6$  absorption at  $n = 5$  (Figure S1). For the  $Cs^+$  ion, the most stable isomer of the  $Cs^+ \cdot (H_2O)_5$  complex has a ring consisting of five  $H_2O$  molecules.<sup>26</sup> This indicates that a five-membered ring is preferred over a four-membered ring for complex formation with  $Cs^+$  ion. The UVPD spectra of the  $Cs^+ \cdot DB18C6 \cdot (H_2O)_n$  complexes show the red-shift from  $n = 0$  up to  $5$ , but the UV absorption shifts to the blue again for  $n = 6$ . The intermolecular interaction of the  $Cs^+$  ion with a six-membered ring is likely to be weaker than that with a five-membered ring. As a result, the interaction of the  $Cs^+$  ion with the  $DB18C6$  component becomes stronger for the  $n = 6$  ion.

**4.5. Hydration Profiles Characteristic of  $M^+ \cdot DB18C6$  ( $M = K, Rb$ , and  $Cs$ ) Complexes.** Figure 1 displays the structures of the  $M^+ \cdot DB18C6 \cdot (H_2O)_{0-5}$  ( $M = K, Rb$ , and  $Cs$ ) complexes determined or tentatively proposed in the previous and present studies.<sup>4,6</sup> The bare complexes,  $M^+ \cdot DB18C6$  ( $M = K, Rb$ , and  $Cs$ ) all adopt the boat conformation (K-a, Rb-a, and Cs-b) in which the cavity of the  $DB18C6$  is most open and the metal ions are located almost at the center of the cavity. The difference in the structure among the bare complexes is the distance between the crown cavity and the metal ions. This small difference leads to a remarkable difference in the structure of the hydrated species. For the  $n = 1$  complexes, the structure is similar for  $K^+$ ,  $Rb^+$ , and  $Cs^+$  (K1a, Rb1a, and Cs1b). For  $n = 2$ ,  $Rb^+$  and  $Cs^+$  complexes have a similar hydration structure (Rb2a and Cs2a); the two  $H_2O$  molecules are bound to  $Rb^+$  or  $Cs^+$  independently and form an  $O-H \cdots \pi$  hydrogen bond. In contrast, the  $K^+ \cdot DB18C6 \cdot (H_2O)_2$  complex has two types of hydration structure, both different from that of the  $Rb^+$  and  $Cs^+$  complexes; the two  $H_2O$  molecules are bound to each other through an  $O-H \cdots O$  hydrogen bond and are located either on top (K2d) or at the bottom (K2f) of the boat-type  $K^+ \cdot DB18C6$  conformer. The  $K^+ \cdot DB18C6 \cdot (H_2O)_3$ ,  $Rb^+ \cdot DB18C6 \cdot (H_2O)_3$ , and  $Cs^+ \cdot DB18C6 \cdot (H_2O)_3$  complexes all have similar hydration structures. One of the two isomers of the  $K^+$  complex (K3a) and the isomers of the  $Rb^+$  and  $Cs^+$  complexes (Rb3a and Cs3a) have all three  $H_2O$  molecules on top of the  $M^+ \cdot DB18C6$  part with a similar hydration structure. The  $K^+ \cdot DB18C6 \cdot$

$(H_2O)_3$  complex has an additional isomer (K3g) with two  $H_2O$  molecules on top and one at the bottom of the boat  $K^+ \cdot DB18C6$  conformer. For the  $n = 4$  and  $5$  complexes, the  $K^+$  and  $Rb^+$  complexes have a similar structure to each other (K4a and Rb4a, and K5a and Rb5a), while the  $Cs^+$  complexes have a different hydration pattern (Cs4a and Cs5a). We display top views of the  $n = 4$  and  $5$  complexes in Figures S9 and S10 of the Supporting Information for a closer look at the difference in the structures. In the case of the  $n = 5$  complexes, one of the five  $H_2O$  molecules is bound to an oxygen atom of the  $DB18C6$  component; we label this  $H_2O$  with “1” and other ones successively with “2–5” in Figure S10. For the  $K^+$  and  $Rb^+$  complexes, the third and fifth  $H_2O$  molecules are close to the benzene rings, forming the  $O-H \cdots \pi$  hydrogen bond. In contrast, the distance between the  $H_2O$  ring and the benzene rings is substantially longer for the  $Cs^+$  complex than that for the  $K^+$  and  $Rb^+$  complexes because the  $Cs^+$  ion is displaced largely from the  $DB18C6$  part.

Because the  $K^+$  ion is encapsulated deeply in the  $DB18C6$  cavity,  $H_2O$  molecules can be bound to the  $K^+$  ion on both sides of the  $K^+ \cdot DB18C6$  complex, which results in multiple isomers in both experiment and theory. For the  $Rb^+$  and  $Cs^+$  ions, the distance between the metal ions and the  $DB18C6$  cavity is slightly larger than in the case of the  $K^+$  ion,<sup>4</sup> which allows  $H_2O$  molecules to interact with the  $Rb^+$  or  $Cs^+$  ion only on top of the  $M^+ \cdot DB18C6$  part, providing a single stable conformer. The existence of multiple isomers for the hydrated  $K^+ \cdot DB18C6$  complexes can contribute to the effective formation of the  $K^+ \cdot DB18C6$  complex and preferential capture of  $K^+$  ion by  $DB18C6$  in solution because of “conformational” entropic effects. These are different from usual entropic effects, which are related to the Gibbs free energy of a single conformation, but the higher the number of complex conformers, the more preferred is the complex formation. In this sense, the results of the  $Rb^+$  and  $Cs^+$  complexes reinforce the uniqueness of  $K^+$  ion in the encapsulation by  $DB18C6$ .

## 5. CONCLUSION

We have measured UVPD spectra of  $K^+ \cdot DB18C6 \cdot (H_2O)_n$ ,  $Rb^+ \cdot DB18C6 \cdot (H_2O)_n$ , and  $Cs^+ \cdot DB18C6 \cdot (H_2O)_n$  ( $n = 1-8$ ) complexes and IR-UV double-resonance spectra of the  $Rb^+ \cdot DB18C6 \cdot (H_2O)_{1-5}$  and  $Cs^+ \cdot DB18C6 \cdot (H_2O)_3$  complexes in a cold, 22-pole ion trap. The structure of dominant forms observed in the experiment has been determined or proposed for all the complexes based on the analysis of the UV and IR spectra. Because conformer-specific, IR-UV dip spectra are not available for all the  $Rb^+ \cdot DB18C6 \cdot (H_2O)_n$  and  $Cs^+ \cdot DB18C6 \cdot (H_2O)_n$  complexes, we cannot exclude completely the possibility of other isomers. However, the IR-UV gain spectra, which provide IR bands of all the isomers in the experiment, are well reproduced by calculated spectra of the most stable isomers for the  $Rb^+$  complexes. This suggests that other higher-energy isomers, if they exist, are not so abundant in the experiment. The bare complexes ( $K^+ \cdot DB18C6$ ,  $Rb^+ \cdot DB18C6$ , and  $Cs^+ \cdot DB18C6$ ) have a similar, boat-type conformation, but the distance between the metal ions and the  $DB18C6$  increases with increasing ion size from  $K^+$  to  $Cs^+$ . This structural difference highly affects the manner in which they are hydrated. In the case of the hydrated  $K^+ \cdot DB18C6$  complexes, the water molecules can be bound on both sides of the boat-type  $K^+ \cdot DB18C6$  structure. In contrast, the  $H_2O$  molecules in the hydrated  $Rb^+ \cdot DB18C6$  and  $Cs^+ \cdot DB18C6$  complexes are located only on top of them. The UV absorption shifts gradually to the



low frequency from  $n = 0$  to 4 for the  $K^+$  and  $Rb^+$  complexes and from  $n = 0$  to 5 for the  $Cs^+$  complex, and then shifts back to the high frequency at  $n = 5$  for  $K^+$  and  $Rb^+$  and at  $n = 6$  for  $Cs^+$ . This spectral trend is related to the stability of the hydrated complexes of these ions,  $M^+(H_2O)_n$ . Addition of one  $H_2O$  molecule to the  $K^+ \cdot DB18C6 \cdot (H_2O)_4$ ,  $Rb^+ \cdot DB18C6 \cdot (H_2O)_4$ , or  $Cs^+ \cdot DB18C6 \cdot (H_2O)_5$  complex makes the interaction between the metal ions and the water clusters attached on the boat-type conformers weaker. As a result, the interaction between DB18C6 and the metal ions becomes stronger, and the UV absorption moves back to higher frequency at  $n = 5$  for the  $K^+$  and  $Rb^+$  complexes and at  $n = 6$  for the  $Cs^+$  complexes. These hydration profiles are characteristic of microhydrated systems, where water molecules are bound to the metal ions cooperatively.<sup>25,26</sup> The  $M^+ \cdot DB18C6$  complexes in aqueous solutions are surrounded by a number of  $H_2O$  molecules on both sides of the boat conformers. However, as can be seen in Figure 1,  $H_2O$  molecules will be preferentially bound on top of the boat conformers for the  $Rb^+ \cdot DB18C6$  and  $Cs^+ \cdot DB18C6$  complexes even in aqueous solutions because they are displaced from the center of the DB18C6 cavity. Because the  $K^+ \cdot DB18C6$  complex can accept  $H_2O$  molecules on both sides of the boat conformation, we propose that multiple conformations will contribute entropically to the high stability of the  $K^+ \cdot DB18C6$  complex in solution and hence the selectivity of DB18C6 for  $K^+$ .

## ■ ASSOCIATED CONTENT

### ■ Supporting Information

The Supporting Information is available free of charge on the ACS Publications website at DOI: 10.1021/acs.jpca.7b12385.

UVPD spectra of the  $K^+ \cdot DB18C6 \cdot (H_2O)_m$ ,  $Rb^+ \cdot DB18C6 \cdot (H_2O)_m$ , and  $Cs^+ \cdot DB18C6 \cdot (H_2O)_n$  ( $n = 0-8$ ) complexes; optimized structures of the hydrated  $K^+ \cdot DB18C6$ ,  $Rb^+ \cdot DB18C6$ , and  $Cs^+ \cdot DB18C6$  complexes calculated at the M05-2X/6-311++G(d,p) level; expanded views of the UVPD spectra of the  $n = 1$  complexes; positions of the origin band in the UVPD spectra and results of TD-DFT calculations; full list of authors of ref 21 (PDF)

## ■ AUTHOR INFORMATION

### Corresponding Author

\*E-mail: y-inokuchi@hiroshima-u.ac.jp. Phone: +81 (Japan)-82-424-7101.

### ORCID

Yoshiya Inokuchi: 0000-0001-7959-5315

Thomas R. Rizzo: 0000-0003-2796-905X

### Notes

The authors declare no competing financial interest.

## ■ ACKNOWLEDGMENTS

This work is partly supported by JSPS KAKENHI Grant no. JP16H04098 and the Swiss National Science Foundation through Grant 200020\_165908 and École Polytechnique Fédérale de Lausanne (EPFL). Y.I. and T.E. thank the support from JSPS through the program "Strategic Young Researcher Overseas Visits Program for Accelerating Brain Circulation". A part of the calculations were performed using Research Center for Computational Science, Okazaki, Japan.

## ■ REFERENCES

- (1) Pedersen, C. J. Cyclic Polyethers and Their Complexes with Metal Salts. *J. Am. Chem. Soc.* **1967**, *89*, 7017–7036.
- (2) Izatt, R. M.; Bradshaw, J. S.; Nielsen, S. A.; Lamb, J. D.; Christensen, J. J.; Sen, D. Thermodynamic and Kinetic Data for Cation Macrocyclic Interaction. *Chem. Rev.* **1985**, *85*, 271–339.
- (3) Izatt, R. M.; Terry, R. E.; Haymore, B. L.; Hansen, L. D.; Dalley, N. K.; Avondet, A. G.; Christensen, J. J. Calorimetric Titration Study of Interaction of Several Univalent and Bivalent-Cations with 15-Crown-5, 18-Crown-6, and Two Isomers of Dicyclohexo-18-Crown-6 in Aqueous-Solution at 25 °C and  $\mu = 0.1$ . *J. Am. Chem. Soc.* **1976**, *98*, 7620–7626.
- (4) Inokuchi, Y.; Boyarkin, O. V.; Kusaka, R.; Haino, T.; Ebata, T.; Rizzo, T. R. UV and IR Spectroscopic Studies of Cold Alkali Metal Ion-Crown Ether Complexes in the Gas Phase. *J. Am. Chem. Soc.* **2011**, *133*, 12256–12263.
- (5) Inokuchi, Y.; Boyarkin, O. V.; Kusaka, R.; Haino, T.; Ebata, T.; Rizzo, T. R. Ion Selectivity of Crown Ethers Investigated by UV and IR Spectroscopy in a Cold Ion Trap. *J. Phys. Chem. A* **2012**, *116*, 4057–4068.
- (6) Inokuchi, Y.; Ebata, T.; Rizzo, T. R.; Boyarkin, O. V. Microhydration Effects on the Encapsulation of Potassium Ion by Dibenzo-18-Crown-6. *J. Am. Chem. Soc.* **2014**, *136*, 1815–1824.
- (7) More, M. B.; Ray, D.; Armentrout, P. B. Cation-Ether Complexes in the Gas Phase: Bond Dissociation Energies of  $M^+(\text{Dimethyl Ether})_x$ ,  $x = 1-3$ ,  $M^+(1,2\text{-Dimethoxyethane})_x$ ,  $x = 1$  and 2, and  $M^+(12\text{-Crown-4})$  Where  $M = Rb$  and  $Cs$ . *J. Phys. Chem. A* **1997**, *101*, 7007–7017.
- (8) More, M. B.; Ray, D.; Armentrout, P. B. Intrinsic Affinities of Alkali Cations for 15-Crown-5 and 18-Crown-6: Bond Dissociation Energies of Gas-Phase  $M^+$ -Crown Ether Complexes. *J. Am. Chem. Soc.* **1999**, *121*, 417–423.
- (9) Rodriguez, J. D.; Lisy, J. M. Infrared Spectroscopy of Gas-Phase Hydrated  $K^+ \cdot 18\text{-Crown-6}$  Complexes: Evidence for High Energy Conformer Trapping Using the Argon Tagging Method. *Int. J. Mass Spectrom.* **2009**, *283*, 135–139.
- (10) Rodriguez, J. D.; Vaden, T. D.; Lisy, J. M. Infrared Spectroscopy of Ionophore-Model Systems: Hydrated Alkali Metal Ion 18-Crown-6 Ether Complexes. *J. Am. Chem. Soc.* **2009**, *131*, 17277–17285.
- (11) Rodriguez, J. D.; Lisy, J. M. Probing Ionophore Selectivity in Argon-Tagged Hydrated Alkali Metal Ion-Crown Ether Systems. *J. Am. Chem. Soc.* **2011**, *133*, 11136–11146.
- (12) Inokuchi, Y.; Ebata, T.; Rizzo, T. R. Solvent Effects on the Encapsulation of Divalent Ions by Benzo-18-Crown-6 and Benzo-15-Crown-5. *J. Phys. Chem. A* **2015**, *119*, 8097–8105.
- (13) Inokuchi, Y.; Ebata, T.; Rizzo, T. R. UV and IR Spectroscopy of Cold  $H_2O^+$ -Benzo-Crown Ether Complexes. *J. Phys. Chem. A* **2015**, *119*, 11113–11118.
- (14) Inokuchi, Y.; Nakatsuma, M.; Kida, M.; Ebata, T. Conformation of Alkali Metal Ion-Benzo-12-Crown-4 Complexes Investigated by UV Photodissociation and UV-UV Hole-Burning Spectroscopy. *J. Phys. Chem. A* **2016**, *120*, 6394–6401.
- (15) Inokuchi, Y.; Kida, M.; Ebata, T. Geometric and Electronic Structures of Dibenzo-15-Crown-5 Complexes with Alkali Metal Ions Studied by UV Photodissociation and UV-UV Hole-Burning Spectroscopy. *J. Phys. Chem. A* **2017**, *121*, 954–962.
- (16) Svendsen, A.; Lorenz, U. J.; Boyarkin, O. V.; Rizzo, T. R. A New Tandem Mass Spectrometer for Photofragment Spectroscopy of Cold, Gas-Phase Molecular Ions. *Rev. Sci. Instrum.* **2010**, *81*, 073107.
- (17) Boyarkin, O. V.; Mercier, S. R.; Kamariotis, A.; Rizzo, T. R. Electronic Spectroscopy of Cold, Protonated Tryptophan and Tyrosine. *J. Am. Chem. Soc.* **2006**, *128*, 2816–2817.
- (18) Rizzo, T. R.; Stearns, J. A.; Boyarkin, O. V. Spectroscopic Studies of Cold, Gas-Phase Biomolecular Ions. *Int. Rev. Phys. Chem.* **2009**, *28*, 481–515.
- (19) Nagornova, N. S.; Rizzo, T. R.; Boyarkin, O. V. Exploring the Mechanism of IR–UV Double-Resonance for Quantitative Spectroscopy of Protonated Polypeptides and Proteins. *Angew. Chem., Int. Ed.* **2013**, *52*, 6002–6005.

(20) Mohamadi, F.; Richards, N. G. J.; Guida, W. C.; Liskamp, R.; Lipton, M.; Caufield, C.; Chang, G.; Hendrickson, T.; Still, W. C. Macromodel - an Integrated Software System for Modeling Organic and Bioorganic Molecules Using Molecular Mechanics. *J. Comput. Chem.* **1990**, *11*, 440–467.

(21) Frisch, M. J.; Trucks, G. W.; Schlegel, H. B.; Scuseria, G. E.; Robb, M. A.; Cheeseman, J. R.; Scalmani, G.; Barone, V.; Mennucci, B.; Petersson, G. A., et al. *Gaussian 09, Revision A.1*; Gaussian, Inc.: Wallingford, CT, 2009.

(22) Schuchardt, K. L.; Didier, B. T.; Elsethagen, T.; Sun, L. S.; Gurumoorathi, V.; Chase, J.; Li, J.; Windus, T. L. Basis Set Exchange: A Community Database for Computational Sciences. *J. Chem. Inf. Model.* **2007**, *47*, 1045–1052.

(23) Kusaka, R.; Inokuchi, Y.; Ebata, T. Laser Spectroscopic Study on the Conformations and the Hydrated Structures of Benzo-18-Crown-6-Ether and Dibenzo-18-Crown-6-Ether in Supersonic Jets. *Phys. Chem. Chem. Phys.* **2007**, *9*, 4452–4459.

(24) Kusaka, R.; Kokubu, S.; Inokuchi, Y.; Haino, T.; Ebata, T. Structure of Host-Guest Complexes between Dibenzo-18-Crown-6 and Water, Ammonia, Methanol, and Acetylene: Evidence of Molecular Recognition on the Complexation. *Phys. Chem. Chem. Phys.* **2011**, *13*, 6827–6836.

(25) Miller, D. J.; Lisy, J. M. Hydrated Alkali-Metal Cations: Infrared Spectroscopy and Ab Initio Calculations of  $M^+(H_2O)_{X=2-5}Ar$  Cluster Ions for  $M = Li, Na, K$ , and  $Cs$ . *J. Am. Chem. Soc.* **2008**, *130*, 15381–15392.

(26) Miller, D. J.; Lisy, J. M. Entropic Effects on Hydrated Alkali-Metal Cations: Infrared Spectroscopy and Ab Initio Calculations of  $M^+(H_2O)_{X=2-5}$  Cluster Ions for  $M = Li, Na, K$ , and  $Cs$ . *J. Am. Chem. Soc.* **2008**, *130*, 15393–15404.